

A randomized algorithm to solve reduced rank operator regression *

Giacomo Turri^{†‡§#}, Vladimir Kostic^{†¶#}, Pietro Novelli^{†#}, and Massimiliano Pontil^{†||}

Abstract. We present and analyze an algorithm designed for addressing vector-valued regression problems involving possibly infinite-dimensional input and output spaces. The algorithm is a randomized adaptation of *reduced rank regression*, a technique introduced in [14] and extended to infinite dimensions in [23] to optimally learn a low-rank vector-valued function (i.e. an operator) between sampled data via regularized empirical risk minimization with rank constraints. We propose Gaussian sketching techniques both for the primal and dual optimization objectives, yielding *Randomized Reduced Rank Regression* (\mathbb{R}^4) estimators that are efficient and accurate. For each of our \mathbb{R}^4 algorithms we prove that the resulting regularized empirical risk is, in expectation w.r.t. randomness of a sketch, arbitrarily close to the optimal value when hyper-parameters are properly tuned. Numerical experiments illustrate the tightness of our bounds and show advantages in two distinct scenarios: (i) solving a vector-valued regression problem using synthetic and large-scale neuroscience datasets, and (ii) regressing the Koopman operator of a nonlinear stochastic dynamical system.

Key words. Reduced-rank regression, vector-valued regression, randomized SVD, kernel methods

MSC codes. 15A03, 15A18, 68W20

1. Introduction. In this work we study the problem of linear operator regression $\mathbf{A} : \mathcal{H} \rightarrow \mathcal{G}$ between Hilbert spaces \mathcal{H} and \mathcal{G} . In particular, we assume that \mathcal{H} and \mathcal{G} are Reproducing Kernel Hilbert Spaces [3] associated to feature maps $\phi : \mathcal{X} \rightarrow \mathcal{H}$ and $\psi : \mathcal{Y} \rightarrow \mathcal{G}$ on the data space \mathcal{X} , respectively. We aim to find low rank solutions to the problem

$$(1.1) \quad \min_{\mathbf{A} \in \text{HS}(\mathcal{H})} \mathbb{E}_{(x,y) \sim \rho} \|\psi(y) - \mathbf{A}\phi(x)\|_{\mathcal{H}}^2.$$

Here $\text{HS}(\mathcal{H})$ is the space of Hilbert-Schmidt operators on \mathcal{H} and ρ is an unknown probability distribution on $\mathcal{X} \times \mathcal{Y}$.

Whenever both ϕ and ψ are the identity functions, (1.1) recover the classical reduced rank regression objective [14]. On the other hand, the full-fledged kernelized version of (1.1) are

* **Funding:** The work is partially funded by the Italian Ministry of University and Research (MUR) through the project PNRR MUR Project PE000013 CUP J53C22003010006 "Future Artificial Intelligence Research (FAIR)" and was carried out within the framework of the project "RAISE - Robotics and AI for Socio-economic Empowerment", both supported by the European Union – NextGenerationEU. However, the views and opinions expressed are those of the authors alone and do not necessarily reflect those of the European Union or the European Commission. Neither the European Union nor the European Commission can be held responsible for them.

[†]Computational Statistics and Machine Learning (CSML) unit, Istituto Italiano di Tecnologia, Genoa, Italy (giacomo.turri@iit.it; vladimir.kostic@iit.it; pietro.novelli@iit.it; massimiliano.pontil@iit.it)

[‡]Unit for Visually Impaired People (U-VIP), Istituto Italiano di Tecnologia, Genoa, Italy

[§]RAISE ecosystem, Genoa, Italy

[¶]University of Novi Sad, Novi Sad, Serbia

^{||}Department of Computer Science and UCL Centre for Artificial Intelligence, University College London, United Kingdom

[#]These authors contributed equally to this work

of interest in the machine learning community, and especially for structured prediction [9], conditional mean embeddings [32] and general linear operator regression [21]. Furthermore, as amply discussed in [16], problems of the form (1.1) naturally arise also in the context of dynamical systems learning, where accurate low-rank solutions provide a succinct and interpretable tool to describe nonlinear dynamical systems via Koopman/Transfer operators.

When a dataset $\mathcal{D}_n = \{(x_i, y_i)\}_{i \in [n]}$ sampled from ρ is available, (1.1) is approximately solved via (regularized) empirical risk minimization (RERM). In this work we consider the following empirical minimization problem

$$(1.2) \quad \mathbf{A}_{r,\gamma} := \arg \min_{\mathbf{A} \in \text{HS}_r(\mathcal{H}, \mathcal{G})} \frac{1}{n} \sum_{i=1}^n \|\psi(y_i) - \mathbf{A}\phi(x_i)\|_{\mathcal{G}}^2 + \gamma \|\mathbf{A}\|_{\text{HS}}^2 := \mathcal{R}^\gamma(\mathbf{A}),$$

where $\text{HS}_r(\mathcal{H}, \mathcal{G}) = \{\mathbf{A} \in \text{HS}(\mathcal{H}, \mathcal{G}) \mid \text{rank}(\mathbf{A}) \leq r\}$, while $r \geq 1$ and $\gamma > 0$ are the rank constraint and regularization parameter, respectively. The estimator (1.2) has been originally proposed in the finite dimensional setting in [14] and recently extended to infinite dimensional spaces in [23, 16].

Notice that in (1.2) two concurrent regularization schemes are considered, the first being a hard constraint on the rank of the estimator and the other being the classical Tikhonov regularization. In this work we provide an algorithm to *efficiently* solve (1.2), eliminating the need to solve large (and potentially non-symmetric) generalized eigenvalue problems arising when dealing with large scale datasets. To that end, we address the *fixed-design* setting, ignoring the randomness of the data \mathcal{D}_n and any statistical-learning-related matters.

Related work. Low rank regression models have wide applications. For instance they have been used for time series analysis and forecasting [8, 30], in chemometrics [23], in multitask learning [2, 7], in structure prediction [19], and to compress parameters in neural networks [13], among others. We also refer to [5, 10, 27] and references therein for related work on low rank regression problems.

Structure of the paper. We introduce the background and setting in Section 2, and define our randomized adaptation of the reduced rank regression estimator in Section 3. In Section 4 we provide error bounds on the risk of the estimators, while in Section 5 we present numerical experiments on synthetic as well as large-scale neuroscience datasets.

Notation. Throughout the paper operators are denoted with bold-face sans-serif fonts (e.g. \mathbf{A}) and matrices with roman fonts (e.g. A). For any operator (or matrix) \mathbf{A} , the orthogonal projector onto $\text{Im}(\mathbf{A})$ is $\pi(\mathbf{A})$. The composition $\mathbf{A} \circ M$ between $\mathbf{A} : \mathbb{R}^n \rightarrow \mathcal{V}$, \mathcal{V} being a possibly infinite dimensional linear space, and $M \in \mathbb{R}^{n \times k}$ is shortened to $\mathbf{A}M$. The r -truncated SVD of Hilbert-Schmidt operators and matrices is denoted by $[\cdot]_r$.

2. Background and preliminaries. Given the data $\mathcal{D}_n := (x_i, y_i)_{i=1}^n$, the *sampling operators* are objects relating the spaces \mathcal{H} and \mathcal{G} to the empirical distribution of data. They are particularly handy in the analysis of the optimization objective (1.2) in either its primal or (convex) dual form [4]. The sampling operators for inputs $\mathbf{S} : \mathcal{H} \rightarrow \mathbb{R}^n$ and outputs $\mathbf{Z} : \mathcal{G} \rightarrow \mathbb{R}^n$ are defined, respectively, as

$$\mathbf{S}h := \frac{1}{\sqrt{n}} [\langle h, \phi(x_i) \rangle_{\mathcal{H}}]_{i \in [n]}, \quad \mathbf{Z}g := \frac{1}{\sqrt{n}} [\langle g, \psi(y_i) \rangle_{\mathcal{G}}]_{i \in [n]}, \quad \text{for all } h \in \mathcal{H}, g \in \mathcal{G}.$$

It is readily verified that their adjoints are given by

$$\mathbf{S}^*v = \frac{1}{\sqrt{n}} \sum_{i \in [n]} v_i \phi(x_i), \quad \mathbf{Z}^*u = \frac{1}{\sqrt{n}} \sum_{i \in [n]} u_i \psi(y_i), \quad \text{for all } u, v \in \mathbb{R}^n.$$

Composing sampling operators one obtains

$$\mathbf{C} := \mathbf{S}^*\mathbf{S} = \frac{1}{n} \sum_{i \in [n]} \phi(x_i) \otimes \phi(x_i), \quad \mathbf{D} := \mathbf{Z}^*\mathbf{Z} = \frac{1}{n} \sum_{i \in [n]} \psi(y_i) \otimes \psi(y_i),$$

the input and output *covariance operators*, respectively, and

$$K := \mathbf{S}\mathbf{S}^* = n^{-1}[k(x_i, x_j)]_{i,j \in [n]}, \quad L := \mathbf{Z}\mathbf{Z}^* = n^{-1}[\ell(y_i, y_j)]_{i,j \in [n]},$$

the input and output *kernel matrices*, respectively. Moreover, the cross-covariance operator $\mathbf{T}: \mathcal{G} \rightarrow \mathcal{H}$ is given by the formula

$$\mathbf{T} := \mathbf{S}^*\mathbf{Z} = \frac{1}{n} \sum_{i \in [n]} \phi(x_i) \otimes \psi(y_i).$$

We conclude with some results on the rank-constrained empirical risk minimization (1.2), omitting the proofs since they are minimal modification of the results in [16].

Proposition 2.1. *For the empirical risk minimization (1.2) the following results hold.*

(1) *For any $\mathbf{A} \in \text{HS}(\mathcal{H}, \mathcal{G})$, the risk defined in (1.2) can be decomposed as*

$$(2.1) \quad \mathcal{R}^\gamma(\mathbf{A}) = \text{tr}(\mathbf{D}) - \|\mathbf{T}^*\mathbf{C}_\gamma^{-\frac{1}{2}}\|_{\text{HS}}^2 + \|\mathbf{A}\mathbf{C}_\gamma^{\frac{1}{2}} - \mathbf{T}^*\mathbf{C}_\gamma^{-\frac{1}{2}}\|_{\text{HS}}^2.$$

(2) *The minimizer $\mathbf{A}_{r,\gamma}$ of (1.2) is*

$$(2.2) \quad \mathbf{A}_{r,\gamma} = \llbracket \mathbf{T}^*\mathbf{C}_\gamma^{-\frac{1}{2}} \rrbracket_r \mathbf{C}_\gamma^{-\frac{1}{2}},$$

where $\mathbf{C}_\gamma := \mathbf{C} + \gamma\mathbf{I}$ is the Tikhonov-regularized input covariance.

(3) *The optimal value of the regularized risk is*

$$(2.3) \quad \mathcal{R}^\gamma(\mathbf{A}_{r,\gamma}) = \text{tr}(\mathbf{D}) - \sum_{i \in [r]} \sigma_i^2,$$

where $\sigma_1 \geq \dots \geq \sigma_r$ are the leading singular values of $\mathbf{T}^*\mathbf{C}_\gamma^{-\frac{1}{2}}$.

For finite dimensional \mathcal{H} and \mathcal{G} , since \mathbf{C}_γ and \mathbf{T} are matrices, the solution $\mathbf{A}_{r,\gamma}$ can be computed by directly evaluating the covariance matrices. Otherwise, one needs to translate the computation to the convex dual using the sampling operators. This is summarized in the following result.

Proposition 2.2. *Denoting the regularized kernel matrix of inputs as $K_\gamma := K + \gamma I$, the operator $\mathbf{A}_{r,\gamma}$ can be represented in the following ways:*

(1) *Primal formulation:* $\mathbf{A}_{r,\gamma} = \mathbf{T}^* \mathbf{H}_r$, where $\mathbf{H}_r := \sum_{i \in [r]} \langle h_i, \mathbf{C}_\gamma h_i \rangle_{\mathcal{H}}^{-1} h_i \otimes h_i$ with $h_i \in \mathcal{H}$ being the r leading eigenvectors of the generalized eigenvalue problem (GEP)

$$(2.4) \quad \mathbf{T} \mathbf{T}^* h_i = \sigma_i^2 \mathbf{C}_\gamma h_i, \quad i \in [r],$$

(2) *Dual formulation:* $\mathbf{A}_{r,\gamma} = \mathbf{Z}^* \widehat{\mathbf{U}}_r \widehat{\mathbf{V}}_r^\top \mathbf{S}$, where $\widehat{\mathbf{U}}_r = K \widehat{\mathbf{V}}_r$ and $\widehat{\mathbf{V}}_r \in \mathbb{R}^{n \times r}$ is the matrix whose columns are the r leading eigenvectors solving the GEP

$$(2.5) \quad LK \widehat{v}_i = \sigma_i^2 K_\gamma \widehat{v}_i, \quad i \in [r]$$

normalized as $\widehat{v}_i^\top K K_\gamma \widehat{v}_i = 1$, $i \in [r]$.

In typical situations when the dimension of the RKHS spaces is very large and one has many samples, the methods above are computationally intensive since large scale symmetric GEP (2.4), or even non-symmetric GEP (2.5) needs to be solved. In the latter case, the situation is often aggravated by L and K being ill-conditioned. In these common scenarios, classical approaches such as the implicitly restarted Arnoldi method, might exhibit slow convergence. In this work we propose an alternative numerical approach by computing the SVD appearing in $\mathbf{A}_{r,\gamma} = \llbracket \mathbf{T}^* \mathbf{C}_\gamma^{-\frac{1}{2}} \rrbracket_r \mathbf{C}_\gamma^{-\frac{1}{2}}$ via a randomized algorithm.

Relying on the classical theory of randomized SVD algorithms for matrices presented in [20], we propose a novel randomized algorithm specialized in solving the RERM (1.2). We also provide error bounds in expectation and show the performance improvement over the current GEP solver. Following Proposition 2.2, we develop our randomized algorithms both for the primal and dual formulations of (1.2). To that end, we rely on the following standard results on linear operators, see e.g. [15].

Fact 1. Let $\mathbf{M} : \mathcal{V} \rightarrow \mathcal{V} = \mathbf{A}^* \mathbf{B}$ with $\mathbf{A}, \mathbf{B} : \mathcal{V} \rightarrow \mathbb{R}^n$, \mathcal{V} being a generic vector space. The eigenvectors h_i of \mathbf{M} corresponding to non-null eigenvalues $\lambda_i \neq 0$ are of the form $h_i = \mathbf{A}^* w_i$ with $w_i \in \mathbb{R}^n$ satisfying the matrix eigenvalue equation

$$\mathbf{B} \mathbf{A}^* w_i = \lambda_i w_i.$$

Fact 2. Let f be a continuous spectral function and \mathbf{A} be a compact linear operator. Then, it holds $\mathbf{A}^* f(\mathbf{A} \mathbf{A}^*) = f(\mathbf{A}^* \mathbf{A}) \mathbf{A}$. In particular, for any $\gamma > 0$ one has $\mathbf{A}^* (\mathbf{A} \mathbf{A}^* + \gamma I)^{-1} = (\mathbf{A}^* \mathbf{A} + \gamma I)^{-1} \mathbf{A}$.

Fact 3. Let $A \in \mathbb{R}^{n \times m}$, $\mathbf{M} : \mathbb{R}^n \rightarrow \mathcal{V}$, \mathcal{V} being a generic vector space. Then, the projector onto the range of $\mathbf{B} \mathbf{A}$ is then given by $\pi(\mathbf{M} \mathbf{A}) = \mathbf{M} \mathbf{W} \mathbf{M}^*$, where $\mathbf{W} = A(A^* \mathbf{M}^* \mathbf{M} A)^\dagger A^* \in \mathbb{R}^{n \times n}$.

Fact 4. Let $A, B \in \mathbb{R}^{n \times n}$ be two symmetric positive semi-definite matrices. Then $(\lambda, q) \in \mathbb{R}_+ \times \mathbb{R}^n$ is a finite eigenpair of $A^\dagger B$ if and only if $Bq = \lambda Aq$ and $q \in \text{Ker}(A)^\perp$.

Finally, we conclude this section with a simple preliminary result used in proving the error bounds. It relates SVD of an operator \mathbf{B} to the SVD of the appropriate matrix B , and is slightly different form can also be found in [22].

Proposition 2.3. Let $\mathbf{B} = \mathbf{S}^* \mathbf{W} \mathbf{Z} : \mathcal{G} \rightarrow \mathcal{H}$ and $B = K^{\frac{1}{2}} \mathbf{W} L^{\frac{1}{2}} \in \mathbb{R}^{n \times n}$. Then $\text{rank}(\mathbf{B}) = \text{rank}(B) =: r$ and there exist $U, V \in \mathbb{R}^{n \times r}$ and a positive diagonal matrix $\Sigma \in \mathbb{R}^{r \times r}$ such

that $\mathbf{B} = \mathbf{S}^*U\Sigma V^*\mathbf{Z}$ and $B = K^{\frac{1}{2}}U\Sigma V^*L^{\frac{1}{2}} \in \mathbb{R}^{n \times n}$. Moreover, the columns of U form a K -orthonormal system, whereas the columns of V are L -orthonormal.

Proof. First observe that $\text{rank}(\mathbf{B}) = \text{rank}(\mathbf{B}^*\mathbf{B})$ and $\text{rank}(B) = \text{rank}(B^*B)$. So, due to Lemma 1 we have

$$\text{rank}(\mathbf{B}) = \text{rank}(\mathbf{Z}^*W^*\mathbf{S}\mathbf{S}^*W\mathbf{Z}) = \text{rank}(\mathbf{Z}\mathbf{Z}^*W^*KW) = \text{rank}(L^{\frac{1}{2}}W^*KWL^{\frac{1}{2}}W) = \text{rank}(B).$$

Now, let the reduced SVD of \mathbf{B} be $\mathbf{B} := \sum_{i \in [r]} \sigma_i \xi_i \otimes \eta_i$, where $(\xi_i)_{i \in [r]} \in \mathcal{H}$ and $(\eta_i)_{i \in [r]} \in \mathcal{G}$ are orthonormal systems and $\sigma_1 \geq \dots \geq \sigma_r > 0$. Then we have that $\mathbf{B}^*\mathbf{B}\eta_i = \sigma_i^2 \eta_i$, $i \in [r]$, and again using Lemma 1, we have that for every $i \in [r]$, $\eta_i = \mathbf{Z}^*v_i$ where $W^*KWLv_i = \sigma_i^2 v_i$. But then $(v_i)_{i \in [r]} \in \mathbb{R}^n$ is a L -orthonormal system, and therefore $(L^{\frac{1}{2}}v_i)_{i \in [r]} \in \mathbb{R}^n$ is an orthonormal system. However, since

$$B^*B(L^{\frac{1}{2}}v_i) = L^{\frac{1}{2}}W^*KWLv_i = \sigma_i^2 L^{\frac{1}{2}}v_i,$$

we conclude that the right singular vectors of B are given by $(L^{\frac{1}{2}}v_i)_{i \in [r]} \in \mathbb{R}^n$. To conclude we use that left singular functions are given by $\xi_i = \frac{1}{\sigma_i} \mathbf{B}\eta_i$, $i \in [r]$, and the claim readily follows. ■

3. Randomized reduced rank regression. The general idea behind the randomized SVD algorithm for matrices is to approximate the space $\text{Im}(B)$ of a target matrix B by a (small) subspace $\text{Im}(M)$ for some random matrix M . One way to construct it is via *powered randomized rangefinder* (see [20, Algorithm 9]) as $M = (BB^*)^p Y$, Y being a low-rank Gaussian matrix. The truncated SVD of B is then approximated as $[[B]]_r \approx [[\pi(M)B]]_r$. In this work, we pursue the same ideas to approximate the r -truncated SVD of the operator $\mathbf{B} := \mathbf{C}_\gamma^{-\frac{1}{2}}\mathbf{T}$ appearing, in its adjoint form, in $\mathbf{A}_{r,\gamma}$. We point out that a naïve extension of randomized SVD algorithms for matrices is not efficient in the present case, as the presence of the square-root of the positive operator \mathbf{C}_γ appearing in \mathbf{B} is too expensive to be computed directly. Thus, we propose a method that is tailored to avoid any explicit calculation of the square-root of positive operators. Square-roots of operators appear in the derivation but will always cancel out in the final results. We now detail every step of the proposed algorithm:

- (1) We define the sketching operator $\mathbf{Y} := \mathbf{C}_\gamma^{-\frac{1}{2}}\mathbf{\Omega}$. Here $\mathbf{\Omega}: \mathbb{R}^{r+s} \rightarrow \mathcal{H}$ can be seen as (semi-infinite) matrix with zero-mean random columns $\omega_1, \dots, \omega_{r+s}$. The integer $r > 0$ is the *target rank*, whereas $s > 0$ is the *oversampling* parameter.
- (2) We construct $\mathbf{M} := (\mathbf{B}\mathbf{B}^*)^p \mathbf{Y}$. Here $p \geq 1$ is an integer corresponding to the number of power iterations performed.
- (3) Basic algebraic manipulations yield that

$$(3.1) \quad \mathbf{M} = \mathbf{C}_\gamma^{\frac{1}{2}}\mathbf{\Omega}_p \quad \text{for} \quad \mathbf{\Omega}_p := \mathbf{C}_\gamma^{-1}(\mathbf{T}\mathbf{T}^*\mathbf{C}_\gamma^{-1})^p \mathbf{\Omega}.$$

- (4) Hence, according to Fact 3, we can express $\pi(\mathbf{M}) = \mathbf{C}_\gamma^{\frac{1}{2}}\mathbf{\Omega}_p(\mathbf{\Omega}_p^*\mathbf{C}_\gamma\mathbf{\Omega}_p)^\dagger \mathbf{\Omega}_p^*\mathbf{C}_\gamma^{\frac{1}{2}}$, and obtain $\pi(\mathbf{M})\mathbf{B} = \mathbf{C}_\gamma^{\frac{1}{2}}\mathbf{\Omega}_p(\mathbf{\Omega}_p^*\mathbf{C}_\gamma\mathbf{\Omega}_p)^\dagger \mathbf{\Omega}_p^*\mathbf{T}$.
- (6) To compute the r -truncated SVD of $\pi(\mathbf{M})\mathbf{B}$ we construct its left singular vectors by solving the eigenvalue equation for the operator $\pi(\mathbf{M})\mathbf{B}\mathbf{B}^*\pi(\mathbf{M})$. Using Lemma 1, the

left singular vectors are of the form $\mathbf{C}_\gamma^{\frac{1}{2}} \boldsymbol{\Omega}_p q_i$, where the vectors $q_i \in \mathbb{R}^{(r+s)}$ satisfy the matrix eigenvalue equation $F_0^\dagger F_1 F_0^\dagger F_0 q_i = \sigma_i^2 q_i$ with

$$F_0 := \boldsymbol{\Omega}_p^* \mathbf{C}_\gamma \boldsymbol{\Omega}_p \quad \text{and} \quad F_1 := \boldsymbol{\Omega}_p^* \mathbf{T} \mathbf{T}^* \boldsymbol{\Omega}_p.$$

(7) From Fact 4, solutions of the matrix eigenvalue equation $F_0^\dagger F_1 F_0^\dagger F_0 q_i = \sigma_i^2 q_i$ solve, as well, the following GEP

$$(3.2) \quad F_1 q_i = \sigma_i^2 F_0 q_i, \quad \text{with} \quad q_i^* F_0 q_i = 1.$$

Upon defining $Q_r := [q_1 | \dots | q_r] \in \mathbb{R}^{(r+s) \times r}$ as the matrix whose columns are the first r leading eigenvectors of (3.2), Fact 3 yields that $\pi(\llbracket \pi(\mathbf{M}) \mathbf{B} \rrbracket_r) = \mathbf{C}_\gamma^{\frac{1}{2}} \mathbf{S}^* \boldsymbol{\Omega}_p Q_r Q_r^* \boldsymbol{\Omega}_p^* \mathbf{C}_\gamma^{\frac{1}{2}}$.

(8) The r -truncated SVD of \mathbf{B} is approximated by

$$(3.3) \quad \llbracket \mathbf{B} \rrbracket_r \approx \llbracket \pi(\mathbf{M}) \mathbf{B} \rrbracket_r = \pi(\llbracket \pi(\mathbf{M}) \mathbf{B} \rrbracket_r) \mathbf{B} = \mathbf{C}_\gamma^{\frac{1}{2}} \boldsymbol{\Omega}_p Q_r Q_r^* \boldsymbol{\Omega}_p^* \mathbf{T}.$$

(9) Finally, plugging (3.3) into $\mathbf{A}_{r,\gamma} = \llbracket \mathbf{B} \rrbracket_r^* \mathbf{C}_\gamma^{-\frac{1}{2}}$, we conclude that

$$(3.4) \quad \mathbf{A}_{r,\gamma}^{s,p} := \mathbf{T}^* \boldsymbol{\Omega}_p Q_r Q_r^* \boldsymbol{\Omega}_p^*.$$

Notice how in the randomized reduced rank regression (\mathbb{R}^4) procedure described above the main computational difficulty lies in obtaining $\boldsymbol{\Omega}_p$ in step (3), while the rest of the algorithm can be efficiently performed in low-dimensional $\mathbb{R}^{(r+s) \times (r+s)}$ space. So, depending on the nature of the spaces \mathcal{H} and \mathcal{G} , we will formalize two variants of the method given above:

- Primal \mathbb{R}^4 algorithm, useful when $\min\{\dim(\mathcal{H}), \dim(\mathcal{G})\} \leq n$,
- Dual \mathbb{R}^4 algorithm, useful when $n < \min\{\dim(\mathcal{H}), \dim(\mathcal{G})\} \leq \infty$.

3.1. Primal \mathbb{R}^4 algorithm. The algorithm in its primal formulation is just a formalization of the ideas of the previous paragraph. This variant is preferable when the number of data samples is larger than the (finite) dimension of at least one feature map ϕ or ψ . In Algorithm 3.1, we detail every step of the algorithm in the case $\dim(\mathcal{H}) \leq \dim(\mathcal{G})$, which can be assumed w.l.o.g. Since in this case

$$(3.5) \quad \mathbf{T} \mathbf{T}^* = \mathbf{S}^* \mathbf{L} \mathbf{S},$$

we can always compute $\mathbf{T} \mathbf{T}^*$, even when \mathcal{G} is infinite dimensional. Further, we write Ω , Ω_p , C_γ and S instead of $\boldsymbol{\Omega}$, $\boldsymbol{\Omega}_p$, \mathbf{C}_γ and \mathbf{S} , respectively, emphasizing that these operators are matrices. Finally, to promote the numerical stability in the computation of projection in step (4), we follow the standard practice [33] of orthonormalizing the basis of the approximate range through economy-size QR decomposition, hereby denoted as `qr_econ`.

3.2. Dual \mathbb{R}^4 algorithm. To address the case $n < \dim(\mathcal{H}) \leq \infty$, the main idea is to construct the sketching operator as $\boldsymbol{\Omega} := \mathbf{S}^* \Omega$, where $\Omega \in \mathbb{R}^{n \times (r+s)}$ is a Gaussian matrix. Before stating the proposed dual algorithm we report a Lemma that gives key insights on how to translate the operator regression problem into an equivalent matrix problem.

Algorithm 3.1 Primal R⁴: $\dim(\mathcal{H}) \leq n$

Require: dataset \mathcal{D}_n , power $p \geq 1$, oversampling $s \geq 2$ and random sketching $\Omega \in \mathbb{R}^{\dim(\mathcal{H}) \times (r+s)}$

- 1: Compute matrix $N = S^*LS \in \mathbb{R}^{\dim(\mathcal{H}) \times \dim(\mathcal{H})}$
- 2: **for** $j \in [p]$ **do**
- 3: Solve $C_\gamma \Omega_p = \Omega$
- 4: Update $\Omega \leftarrow N\Omega_p$
- 5: Compute $\Omega, _ = \text{qr_econ}(\Omega)$
- 6: **end for**
- 7: Solve $C_\gamma \Omega_p = \Omega$
- 8: Compute $F_0 = \Omega_p^* \Omega$ and $F_1 = \Omega_p^*(N\Omega_p)$
- 9: Compute the r leading eigenpairs (σ_i^2, q_i) of $F_1 q_i = \sigma_i^2 F_0 q_i$
- 10: Update $q_i \leftarrow q_i / \sqrt{q_i^* F_0 q_i}$
- 11: Compute $\widehat{V}_{r,p} = \Omega_p Q_r$, for $Q_r = [q_1 \dots q_r] \in \mathbb{R}^{(r+s) \times r}$

Ensure: $\mathbf{A}_{r,\gamma}^{s,p} := \mathbf{T}^* \widehat{V}_{r,p} \widehat{V}_{r,p}^*$

Lemma 3.1. *Let $p \geq 1$. Given $\Omega \in \mathbb{R}^{n \times k}$, let $\mathbf{\Omega} = \mathbf{S}^* \Omega$. Then, recalling that $\mathbf{B} := \mathbf{C}_\gamma^{-\frac{1}{2}} \mathbf{T}$, $\mathbf{Y} := \mathbf{C}_\gamma^{-\frac{1}{2}} \mathbf{\Omega}$ and (3.1), for matrices $B := K^{\frac{1}{2}} K_\gamma^{-\frac{1}{2}} L^{\frac{1}{2}}$, $Y := K_\gamma^{-\frac{1}{2}} K^{\frac{1}{2}} \Omega$, $\Omega_p := K_\gamma^{-1} (L(I_n - \gamma K_\gamma^{-1}))^p \Omega$ and $M := (BB^*)^p Y$ it holds that*

$$(3.6) \quad \mathbf{\Omega}_p = \mathbf{S}^* \Omega_p, \quad \|\llbracket \mathbf{B} \rrbracket_r\|_{\text{HS}}^2 = \|\llbracket B \rrbracket_r\|_F^2 \quad \text{and} \quad \|\pi(\mathbf{M}) \llbracket \mathbf{B} \rrbracket_r\|_{\text{HS}}^2 = \|\pi(Y) \llbracket B \rrbracket_r\|_F^2.$$

Proof. Since $\mathbf{B} = \mathbf{C}_\gamma^{-\frac{1}{2}} \mathbf{T} = \mathbf{S} K_\gamma^{-\frac{1}{2}} \mathbf{Z}$, from Proposition 2.3 we have that reduced SVD of \mathbf{B} and B can be expressed as $\llbracket \mathbf{B} \rrbracket_r = \mathbf{S} \mathbf{U} \Sigma \mathbf{V}^* \mathbf{Z}$ and $\llbracket B \rrbracket_r = K^{\frac{1}{2}} U \Sigma V^* L^{\frac{1}{2}}$, respectively. But then, clearly $\|\llbracket \mathbf{B} \rrbracket_r\|_{\text{HS}}^2 = \|\llbracket B \rrbracket_r\|_F^2 = \sum_{i \in [r]} \sigma_i^2$.

Next, since

$$M = (BB^*)^p Y = (K^{\frac{1}{2}} K_\gamma^{-\frac{1}{2}} L K_\gamma^{-\frac{1}{2}} K^{\frac{1}{2}})^p K_\gamma^{-\frac{1}{2}} K^{\frac{1}{2}} \Omega = K^{\frac{1}{2}} K_\gamma^{-\frac{1}{2}} (L K K_\gamma^{-1})^p \Omega,$$

recalling $\Omega_p = K_\gamma^{-1} (L(I_n - \gamma K_\gamma^{-1}))^p \Omega = K_\gamma^{-1} (L K K_\gamma^{-1})^p \Omega$, we can write $M = K_\gamma^{\frac{1}{2}} K^{\frac{1}{2}} \Omega_p$. In a similar way, we have that for the operator \mathbf{M} holds

$$\mathbf{M} = (\mathbf{B} \mathbf{B}^*)^p \mathbf{Y} = (\mathbf{S}^* K_\gamma^{-\frac{1}{2}} L K_\gamma^{-\frac{1}{2}} \mathbf{S})^p \mathbf{C}_\gamma^{-\frac{1}{2}} \mathbf{S}^* \Omega = \mathbf{S}^* K_\gamma^{-\frac{1}{2}} (L K K_\gamma^{-1})^p \Omega = \mathbf{C}_\gamma^{\frac{1}{2}} \mathbf{S}^* \Omega_p,$$

and, hence $\mathbf{\Omega}_p = \mathbf{S}^* \Omega_p$. Now, let V_r be V truncated to its first r -columns. Then we have $\mathbf{P}_r = \mathbf{Z}^* V_r V_r^* \mathbf{Z}$, and hence $\llbracket \mathbf{B} \rrbracket_r = \mathbf{S}^* K_\gamma^{-\frac{1}{2}} L V_r V_r^* \mathbf{Z}$. Similarly $\llbracket B \rrbracket_r = B L^{\frac{1}{2}} V_r V_r^* L^{\frac{1}{2}} = K^{\frac{1}{2}} K_\gamma^{-\frac{1}{2}} L V_r V_r^* L^{\frac{1}{2}}$. Therefore, it follows

$$\begin{aligned} \mathbf{S} \pi(\mathbf{M}) \mathbf{S}^* &= \mathbf{S} \mathbf{M} (\mathbf{M}^* \mathbf{M})^\dagger \mathbf{M}^* \mathbf{S}^* \\ &= \mathbf{S} \mathbf{C}_\gamma^{\frac{1}{2}} \mathbf{S}^* \Omega_p (\Omega_p^* \mathbf{S} \mathbf{C}_\gamma \mathbf{S}^* \Omega_p)^\dagger \Omega_p^* \mathbf{S} \mathbf{C}_\gamma^{\frac{1}{2}} \mathbf{S}^* \\ &= K K_\gamma^{\frac{1}{2}} \Omega_p (\Omega_p^* K K_\gamma \Omega_p)^\dagger \Omega_p^* K_\gamma^{\frac{1}{2}} K \end{aligned}$$

Algorithm 3.2 Dual R^4 : $n < \dim(\mathcal{H}) \wedge \dim(\mathcal{G}) \leq \infty$

Require: dataset \mathcal{D}_n , power $p \geq 1$, oversampling $s \geq 2$ and random sketching $\Omega \in \mathbb{R}^{n \times (r+s)}$

- 1: **for** $j \in [p]$ **do**
 - 2: Solve $K_\gamma \Omega_p = \Omega$
 - 3: Update $\Omega \leftarrow L(\Omega - \gamma \Omega_p)$
 - 4: Compute $\Omega, _ = \text{qr_econ}(\Omega)$
 - 5: **end for**
 - 6: Solve $K_\gamma \Omega_p = \Omega$
 - 7: Compute $F_0 = \Omega_p^* K \Omega$
 - 8: Update $\Omega \leftarrow L(\Omega - \gamma \Omega_p)$
 - 9: Compute $F_1 = \Omega_p^* K \Omega$
 - 10: Compute the r leading eigenpairs (σ_i^2, q_i) of $F_1 q_i = \sigma_i^2 F_0 q_i$
 - 11: Update $q_i \leftarrow q_i / \sqrt{q_i^* F_0 q_i}$
 - 12: Compute $\widehat{V}_{r,p} = \Omega_p Q_r$, for $Q_r = [q_1 \dots q_r] \in \mathbb{R}^{(r+s) \times r}$
 - 13: Compute $\widehat{U}_{r,p} = K \widehat{V}_{r,p}$
- Ensure:** $\mathbf{A}_{r,\gamma}^{s,p} := \mathbf{Z}^* \widehat{U}_{r,p} \widehat{V}_{r,p}^* \mathbf{S}$
-

$$\begin{aligned}
&= K^{\frac{1}{2}} M (M^* M)^\dagger M^* K^{\frac{1}{2}} \\
&= K^{\frac{1}{2}} \pi(M) K^{\frac{1}{2}},
\end{aligned}$$

and, consequently,

$$\begin{aligned}
\|\pi(\mathbf{M})[\mathbf{B}]_r\|_{\text{HS}}^2 &= \text{tr}([\mathbf{B}]_r^* \pi(\mathbf{M})^2 [\mathbf{B}]_r) \\
&= \text{tr}\left(\mathbf{Z}^* V_r V_r^* L K_\gamma^{-\frac{1}{2}} \mathbf{S} \pi(\mathbf{M}) \mathbf{S}^* K_\gamma^{-\frac{1}{2}} L V_r V_r^* \mathbf{Z}\right) \\
&= \text{tr}\left(\mathbf{Z} \mathbf{Z}^* V_r V_r^* L^{\frac{1}{2}} B^* \pi(M) B L^{\frac{1}{2}} V_r V_r^*\right) \\
&= \text{tr}\left(L V_r V_r^* L^{\frac{1}{2}} B^* \pi(M) B L^{\frac{1}{2}} V_r V_r^*\right) \\
&= \text{tr}\left(L^{\frac{1}{2}} V_r V_r^* L^{\frac{1}{2}} B^* \pi(M)^2 B L^{\frac{1}{2}} V_r V_r^* L^{\frac{1}{2}}\right) \\
&= \|\pi(M)[B]_r\|_F^2.
\end{aligned}$$

concluding the proof. ■

Now, recalling that $\mathbf{A}_{r,\gamma}^{s,p} : \mathbf{T}^* \Omega_p Q_r Q_r^* \Omega_p^* = \mathbf{Z}^* \mathbf{S} \mathbf{S}^* \Omega_p Q_r Q_r^* \Omega_p^* \mathbf{S} = \mathbf{Z}^* K \Omega_p Q_r Q_r^* \Omega_p^* \mathbf{S}$, the dual R^4 , given in Algorithm 3.2, readily follows.

We conclude this section with a remark on computational complexity of R^4 implementations. Recalling Proposition 2.2, one sees that the computational cost of R^4 is fixed a-priori by the choice of s and p , while solving GEP in (2.4) depends on the convergence rate of the generalized eigenvalue solver of choice.

In the following section, we show that the regularized empirical risk of R^4 estimator exhibits fast convergence to the optimal value as the parameters s and p increase.

4. Error bounds. In this section we provide bounds for $\mathbb{E}[\mathcal{R}^\gamma(\mathbf{A}_{r,\gamma}^{s,p})] - \mathcal{R}^\gamma(\mathbf{A}_{r,\gamma})$. Here, the expectation value is intended over the Gaussian matrix Ω appearing in Algorithms 3.1 and 3.2. The main conclusion is that $\mathbb{E}[\mathcal{R}^\gamma(\mathbf{A}_{r,\gamma}^{s,p})] - \mathcal{R}^\gamma(\mathbf{A}_{r,\gamma})$ can be made arbitrarily small by increasing the oversampling $s \geq 2$ and powering $p \geq 1$ parameters. Moreover, when the singular values of B have a rapid decay, the bound is tight already for small values of s and p , e.g, $s \in [r]$ and $p \in [3]$.

The proofs rely on the following proposition linking the randomized SVD of operators to recently developed error analysis for randomized low-rank approximation methods for matrices in [11], which we restate in notation adapted to our manuscript.

Proposition 4.1. *Given $p \geq 1$, $s \geq 2$, data $\mathcal{D} := \{(x_i, y_i)\}_{i \in [n]}$ and operator $\mathbf{\Omega}: \mathbb{R}^{r+s} \rightarrow \mathcal{H}$, for $\mathbf{A}_{r,\gamma}^{s,p}$ given in 3.4 it holds that*

$$(4.1) \quad \mathcal{R}^\gamma(\mathbf{A}_{r,\gamma}^{s,p}) - \mathcal{R}^\gamma(\mathbf{A}_{r,\gamma}) \leq \|(\mathbf{I}_{\mathcal{H}} - \pi(\mathbf{M}))\llbracket \mathbf{B} \rrbracket_r\|_{\text{HS}}^2.$$

Proof. Let us start by recalling that due to (2.2), the minimizer of (1.2) is $\mathbf{A}_{r,\gamma} = \llbracket \mathbf{B} \rrbracket_r^* \mathbf{C}_\gamma^{-\frac{1}{2}}$ while according to (3.3) its randomized approximation is $\mathbf{A}_{r,\gamma}^{s,p} = (\pi(\llbracket \pi(\mathbf{M})\mathbf{B} \rrbracket_r) \mathbf{B})^* \mathbf{C}_\gamma^{-\frac{1}{2}}$. Therefore, (2.1) implies

$$\begin{aligned} \mathcal{R}^\gamma(\mathbf{A}_{r,\gamma}^{s,p}) - \mathcal{R}^\gamma(\mathbf{A}_{r,\gamma}) &= \|\mathbf{A}_{r,\gamma}^{s,p} \mathbf{C}_\gamma^{\frac{1}{2}} - \mathbf{T}^* \mathbf{C}_\gamma^{-\frac{1}{2}}\|_{\text{HS}}^2 - \|\mathbf{A}_{r,\gamma} \mathbf{C}_\gamma^{\frac{1}{2}} - \mathbf{T}^* \mathbf{C}_\gamma^{-\frac{1}{2}}\|_{\text{HS}}^2 \\ &= \|(\pi(\llbracket \pi(\mathbf{M})\mathbf{B} \rrbracket_r) \mathbf{B})^* - \mathbf{B}^*\|_{\text{HS}}^2 - \|\llbracket \mathbf{B}^* \rrbracket_r - \mathbf{B}^*\|_{\text{HS}}^2 \\ &= \|(\mathbf{I}_{\mathcal{H}} - \pi(\llbracket \pi(\mathbf{M})\mathbf{B} \rrbracket_r)) \mathbf{B}\|_{\text{HS}}^2 - \|\llbracket \mathbf{B} \rrbracket_r - \mathbf{B}\|_{\text{HS}}^2 \\ &= \|\mathbf{B}\|_{\text{HS}}^2 - \|\pi(\llbracket \pi(\mathbf{M})\mathbf{B} \rrbracket_r) \mathbf{B}\|_{\text{HS}}^2 - \|\mathbf{B}\|_{\text{HS}}^2 + \|\llbracket \mathbf{B} \rrbracket_r\|_{\text{HS}}^2 \\ &= \|\llbracket \mathbf{B} \rrbracket_r\|_{\text{HS}}^2 - \|\pi(\llbracket \pi(\mathbf{M})\mathbf{B} \rrbracket_r) \mathbf{B}\|_{\text{HS}}^2 \\ &= \|(\mathbf{I}_{\mathcal{H}} - \pi(\mathbf{M}))\llbracket \mathbf{B} \rrbracket_r\|_{\text{HS}}^2 + \|\pi(\mathbf{M})\llbracket \mathbf{B} \rrbracket_r\|_{\text{HS}}^2 - \|\pi(\llbracket \pi(\mathbf{M})\mathbf{B} \rrbracket_r) \mathbf{B}\|_{\text{HS}}^2. \end{aligned}$$

We now show the upper-bound $\|\pi(\mathbf{M})\llbracket \mathbf{B} \rrbracket_r\|_{\text{HS}}^2 \leq \|\pi(\llbracket \pi(\mathbf{M})\mathbf{B} \rrbracket_r) \mathbf{B}\|_{\text{HS}}^2$. Indeed, observe that by (3.3) it holds $\pi(\llbracket \pi(\mathbf{M})\mathbf{B} \rrbracket_r) \mathbf{B} = \llbracket \pi(\mathbf{M})\mathbf{B} \rrbracket_r$. So, denoting by \mathbf{P}_r the projector on the subspace of r leading right singular vectors of \mathbf{B} , we have that

$$\begin{aligned} \|\pi(\mathbf{M})\llbracket \mathbf{B} \rrbracket_r\|_{\text{HS}}^2 - \|\pi(\llbracket \pi(\mathbf{M})\mathbf{B} \rrbracket_r) \mathbf{B}\|_{\text{HS}}^2 &= \|\pi(\mathbf{M})\llbracket \mathbf{B} \rrbracket_r\|_{\text{HS}}^2 - \|\llbracket \pi(\mathbf{M})\mathbf{B} \rrbracket_r\|_{\text{HS}}^2 \\ &= \|\pi(\mathbf{M})\mathbf{B}\mathbf{P}_r\|_{\text{HS}}^2 - \|\llbracket \pi(\mathbf{M})\mathbf{B} \rrbracket_r\|_{\text{HS}}^2 \\ &= \|\pi(\mathbf{M})\mathbf{B}\|_{\text{HS}}^2 - \|\pi(\mathbf{M})\mathbf{B}(\mathbf{I}_{\mathcal{G}} - \mathbf{P}_r)\|_{\text{HS}}^2 - \|\llbracket \pi(\mathbf{M})\mathbf{B} \rrbracket_r\|_{\text{HS}}^2 \\ &= \|\pi(\mathbf{M})\mathbf{B} - \llbracket \pi(\mathbf{M})\mathbf{B} \rrbracket_r\|_{\text{HS}}^2 - \|\pi(\mathbf{M})(\mathbf{B} - \llbracket \mathbf{B} \rrbracket_r)\|_{\text{HS}}^2. \end{aligned}$$

But since $\text{rank}(\pi(\mathbf{M})\llbracket \mathbf{B} \rrbracket_r) \leq \text{rank}(\llbracket \mathbf{B} \rrbracket_r) \leq r$, using the Eckart–Young–Mirsky theorem we have that

$$\begin{aligned} \|\pi(\mathbf{M})\mathbf{B} - \llbracket \pi(\mathbf{M})\mathbf{B} \rrbracket_r\|_{\text{HS}}^2 &= \min_{\tilde{\mathbf{B}} \in \text{HS}_r(\mathcal{H}, \mathcal{G})} \|\pi(\mathbf{M})\mathbf{B} - \tilde{\mathbf{B}}\|_{\text{HS}}^2 \\ &\leq \|\pi(\mathbf{M})(\mathbf{B} - \llbracket \mathbf{B} \rrbracket_r)\|_{\text{HS}}^2, \end{aligned}$$

which concludes the proof. ■

Theorem 4.2 (Theorem 3.17 and Remark 3.18 of [11]). *Given $B \in \mathbb{R}^{m \times n}$ such that $m \geq n$, let $B = U\Sigma V^*$ be its full SVD, $[[B]]_r = U_r \Sigma_r V_r^*$ its r -truncated SVD, for some $r \in [n]$ and let $U = [U_r \ U_{\perp,r}]$. Let $M \in \mathbb{R}^{n \times (r+s)}$, $s \geq 2$, be a Gaussian matrix such that $M \sim \mathcal{N}(0, G)$, where $G \in \mathbb{R}^{n \times n}$ is a covariance matrix. If $G_r := U_r^* G U_r$ is nonsingular, then*

$$(4.2) \quad \mathbb{E} \|[I - \pi(M)][[B]]_r\|_F^2 \leq \min \left\{ \frac{r a_r}{r + a_r} \|B\|^2, b_r \right\},$$

where

$$(4.3) \quad a_r := \text{tr}(G_{\perp,r} G_r^{-2} G_{\perp,r}^*) + \frac{\text{tr}(G_r - G_{\perp,r} G_r^{-1} G_{\perp,r}^*) \text{tr}(G_r^{-1})}{s-1},$$

$$(4.4) \quad b_r := \text{tr}(G_{\perp,r} G_r^{-1} \Sigma_r^2 G_r^{-1} G_{\perp,r}^*) + \frac{\text{tr}(G_r - G_{\perp,r} G_r^{-1} G_{\perp,r}^*) \text{tr}(\Sigma_r G_r^{-1} \Sigma_r)}{s-1},$$

$$G_{\perp,r} := U_r^* G U_r \quad \text{and} \quad \underline{G}_r := U_r^* G U_r.$$

Now, collecting Lemma 3.1, Proposition 4.1 and Theorem 4.2, we immediately obtain the following expected error bound for the randomized reduced rank estimator 3.4.

Theorem 4.3. *Given data $\mathcal{D} := \{(x_i, y_i)\}_{i \in [n]}$, $p \geq 1$ and $s \geq 2$, let $r \leq \text{rank}(\mathbf{T})$ and $\Omega \in \mathbb{R}^{n \times (r+s)}$ be with i.i.d. columns from $\mathcal{N}(0, L)$. If $\Omega = \mathbf{S}^* \Omega$, then, for the randomized reduced rank estimator $\mathbf{A}_{r,\gamma}^{s,p}$ given in 3.4 it holds that*

$$(4.5) \quad \mathbb{E}[\mathcal{R}^\gamma(\mathbf{A}_{r,\gamma}^{s,p})] - \mathcal{R}^\gamma(\mathbf{A}_{r,\gamma}) \leq \min \left\{ \frac{r a_r}{r + a_r} \sigma_1^2, b_r \right\},$$

where

$$(4.6) \quad a_r := \frac{1}{s-1} \left[\sum_{i=r+1}^n \left(\frac{\sigma_i}{\sigma_{r+1}} \right)^{4p+2} \right] \left[\sum_{i=1}^r \left(\frac{\sigma_{r+1}}{\sigma_i} \right)^{4p+2} \right],$$

$$(4.7) \quad b_r := \frac{\sigma_{r+1}^2}{s-1} \left[\sum_{i=r+1}^n \left(\frac{\sigma_i}{\sigma_{r+1}} \right)^{4p+2} \right] \left[\sum_{i=1}^r \left(\frac{\sigma_{r+1}}{\sigma_i} \right)^{4p} \right],$$

and $\sigma_1 \geq \dots \geq \sigma_n$ are singular values of $\mathbf{B} = \mathbf{C}_\gamma^{-\frac{1}{2}} \mathbf{T}$.

Proof. First, observe that Proposition 4.1 guarantees that almost surly

$$\mathcal{R}^\gamma(\mathbf{A}_{r,\gamma}^{s,p}) - \mathcal{R}^\gamma(\mathbf{A}_{r,\gamma}) \leq \|(\mathbf{I}_n - \pi(\mathbf{M}))[[\mathbf{B}]]_r\|_{\text{HS}}^2 = \|[[\mathbf{B}]]_r\|_{\text{HS}}^2 - \|\pi(\mathbf{M})[[\mathbf{B}]]_r\|_{\text{HS}}^2.$$

Hence, due to Lemma 3.1,

$$(4.8) \quad \mathcal{R}^\gamma(\mathbf{A}_{r,\gamma}^{s,p}) - \mathcal{R}^\gamma(\mathbf{A}_{r,\gamma}) \leq \|[[B]]_r\|_F^2 - \|\pi(M)[[B]]_r\|_F^2 = \|(I_n - \pi(M))[[B]]_r\|_F^2.$$

Next, since $L = \mathbb{E}[\Omega\Omega^*]$, the covariance of the random matrix M is

$$(4.9) \quad G = \mathbb{E}[MM^*] = (BB^*)^p K^{\frac{1}{2}} K_\gamma^{-\frac{1}{2}} \mathbb{E}[\Omega\Omega^*] K_\gamma^{-\frac{1}{2}} K^{\frac{1}{2}} (BB^*)^p = (BB^*)^{2p+1}.$$

Hence, the projected covariance becomes $G_r = (K^{\frac{1}{2}}U_r)^*(BB^*)^{2p+1}(K^{\frac{1}{2}}U_r) = \Sigma_r^{4p+2}$. Since, $r \leq \text{rank}(\mathbf{T}^*\mathbf{T}) = \text{rank}(\mathbf{B})$, G_r is nonsingular, and (4.5) holds with a_r and b_r computed according to (4.3) and (4.4), respectively. Using that $G_{\perp,r} = 0$ and $\underline{G}_r = \underline{\Sigma}_r^{4p+2}$, where $\underline{\Sigma}_r = \text{diag}(\sigma_{r+1}, \dots, \sigma_n)$, direct computation yields (4.6) and (4.7). \blacksquare

While the previous theorem provides the bound that quickly becomes zero by increasing s and p , the main downside lies in the fact that generating anisotropic Gaussian sketch $\Omega \sim \mathcal{N}(0, L)$ in certain cases can be computationally expensive. Namely, we have the following:

Corollary 4.4. *Given data $\mathcal{D} := \{(x_i, y_i)\}_{i \in [n]}$, $p \geq 1$ and $s \geq 2$, let $r \leq \text{rank}(\mathbf{T})$. Then, the following holds*

1. *Let $\dim(\mathcal{G}) < \infty$. If $\tilde{\omega}_i \in \mathbb{R}^{\dim(\mathcal{G})}$, $i \in [r+s]$, are i.i.d. from $\mathcal{N}(0, I_{\dim(\mathcal{H})})$ and $\Omega = [T\tilde{\omega}_1 | \dots | T\tilde{\omega}_{r+s}]$, then primal R^4 Algorithm 3.1 produces $\mathbf{A}_{r,\gamma}^{s,p}$ so that (4.5) holds true.*
2. *Let $\dim(\mathcal{G}) = \infty$, and let $N = R\Lambda R^*$ be eigenvalue decomposition of matrix $N = \mathbf{T}\mathbf{T}^* \in \mathbb{R}^{\dim(\mathcal{H}) \times \dim(\mathcal{H})}$. If $\tilde{\omega}_i \in \mathbb{R}^{\dim(\mathcal{G})}$, $i \in [r+s]$, are i.i.d. from $\mathcal{N}(0, I_{\dim(\mathcal{H})})$ and $\Omega = [R\Lambda^{\frac{1}{2}}\tilde{\omega}_1 | \dots | R\Lambda^{\frac{1}{2}}\tilde{\omega}_{r+s}]$, then primal R^4 Algorithm 3.1 produces $\mathbf{A}_{r,\gamma}^{s,p}$ so that (4.5) holds true.*
3. *Let $L = R^*R$ be Cholesky factorization. If $\tilde{\omega}_i \in \mathbb{R}^n$, $i \in [r+s]$, are i.i.d. from $\mathcal{N}(0, I_n)$ and $\Omega = [R^*\tilde{\omega}_1 | \dots | R^*\tilde{\omega}_{r+s}]$, then dual R^4 Algorithm 3.2 produces $\mathbf{A}_{r,\gamma}^{s,p}$ so that (4.5) holds true.*

Therefore, if we have $\dim(\mathcal{H}) \ll n$, we can efficiently apply primal R^4 algorithm with appropriate sketching to obtain strong guarantees of Theorem 4.3. Otherwise, implementing the sketch in Corollary 4.4 becomes too expensive. So, in the following result, we prove that dual R^4 algorithm can provably attain arbitrary small errors even using isotropic Gaussian sketch $\Omega \sim \mathcal{N}(0, I_n)$.

Theorem 4.5. *Given data $\mathcal{D} := \{(x_i, y_i)\}_{i \in [n]}$, if $r \leq \text{rank}(KL)$, $p \geq 1$, $s \geq 2$ and $\Omega \in \mathbb{R}^{n \times (r+s)}$ with iid columns from $\mathcal{N}(0, I_n)$, then for the output $\mathbf{A}_{r,\gamma}^{s,p}$ of the dual R^4 Algorithm 3.2 it holds that*

$$(4.10) \quad \mathbb{E}[\mathcal{R}^\gamma(\mathbf{A}_{r,\gamma}^{s,p})] - \mathcal{R}^\gamma(\mathbf{A}_{r,\gamma}) \leq \min \left\{ \frac{ra_r}{r+a_r} \sigma_1^2, b_r \right\},$$

where

$$(4.11) \quad a_r := \frac{\|L\|}{\sigma_r^2} \left[\sum_{i=r+1}^n \left(\frac{\sigma_i}{\sigma_r} \right)^{4p} \right] \left[1 + \frac{1}{s-1} \sum_{i=1}^r \left(\frac{\sigma_r}{\sigma_i} \right)^{4p+2} \right],$$

$$(4.12) \quad b_r := \|L\| \left[\sum_{i=r+1}^n \left(\frac{\sigma_i}{\sigma_r} \right)^{4p} \right] \left[\frac{\sigma_1^2}{\sigma_r^2} + \frac{1}{s-1} \sum_{i=1}^r \left(\frac{\sigma_r}{\sigma_i} \right)^{4p} \right],$$

and $\sigma_1 \geq \dots \geq \sigma_n$ are singular values of $\mathbf{B} = \mathbf{C}_\gamma^{-\frac{1}{2}}\mathbf{T}$.

Proof. Noting that $\text{rank}(KL) = \text{rank}(\mathbf{B})$, the only difference from the proof of Theorem 4.3 is in the derivation of the bound from (4.8). The difficulty in this case lies in the fact that

since

$$(4.13) \quad G = \mathbb{E}[MM^*] = (BB^*)^p KK_\gamma(BB^*)^p,$$

in general, the projected covariance $G_{\perp,r} \neq 0$. Hence, it is not evident that the first terms in (4.3) and (4.4) can be made arbitrarily small. To address this, observe that $I_n \succeq I_n - \gamma K_\gamma^{-1} = KK_\gamma^{-1}$ and $L \preceq \|L\|I_n$ implies

$$(4.14) \quad \|L\|^{-1}(BB^*)^{2p+1} \preceq G \preceq (BB^*)^{2p}.$$

Moreover, the projected covariance is positive definite, since

$$(4.15) \quad G_r = (K^{\frac{1}{2}}U_r)^*G(K^{\frac{1}{2}}U_r) \succeq \|L\|^{-1}(K^{\frac{1}{2}}U_r)^*(BB^*)^{2p+1}(K^{\frac{1}{2}}U_r) \succeq \|L\|^{-1}\Sigma_r^{4p+2} \succ 0,$$

which implies that its Schur complement w.r.t. to the first r indices $\underline{G}_r - G_{\perp,r}G_r^{-1}G_{\perp,r}^*$ is positive semi-definite. Hence, we obtain $G_{\perp,r}G_r^{-1}G_{\perp,r}^* \preceq \underline{G}_r$. However, projecting (4.14) yields $\underline{G}_r \preceq \Sigma_r^{4p}$, which implies that $G_r^{-1} \preceq \|L\|\Sigma_r^{-4p-2}$ and

$$(4.16) \quad G_{\perp,r}G_r^{-2}G_{\perp,r}^* \preceq \|G_r^{-1}\|G_{\perp,r}G_r^{-1}G_{\perp,r}^* \preceq \|L\|\|\Sigma_r^{-4p-2}\|\underline{G}_r \preceq \frac{\|L\|}{\sigma_r^{4p+2}}\Sigma_r^{4p}.$$

Taking the trace we conclude that

$$(4.17) \quad \text{tr}(G_{\perp,r}G_r^{-2}G_{\perp,r}^*) \leq \frac{\|L\|}{\sigma_r^2} \sum_{i=r+1}^n \left(\frac{\sigma_i}{\sigma_r}\right)^{4p}$$

In a similar manner, we obtain

$$(4.18) \quad \text{tr}(G_{\perp,r}G_r^{-1}\Sigma_r^2G_r^{-1}G_{\perp,r}^*) \leq \|L\|\frac{\sigma_1^2}{\sigma_r^2} \sum_{i=r+1}^n \left(\frac{\sigma_i}{\sigma_r}\right)^{4p},$$

$$(4.19) \quad \text{tr}(G_r^{-1}) \leq \|L\| \sum_{i=1}^r \frac{1}{\sigma_i^{4p+2}} \quad \text{and} \quad \text{tr}(\Sigma_r G_r^{-1} \Sigma_r) \leq \|L\| \sum_{i=1}^r \frac{1}{\sigma_i^{4p}},$$

and (4.11) and (4.12) follow using that $\text{tr}(\underline{G}_r - G_{\perp,r}G_r^{-1}G_{\perp,r}^*) \leq \text{tr}(\Sigma_r^{4p}) = \sum_{i=r+1}^n \sigma_i^{4p}$. ■

As a final remark of this section note that $\sigma_{r+1} < \sigma_r$ suffices to assure that a_r and b_r from (4.11) and (4.12), respectively, converge to zero with the linear rate $(\sigma_{r+1}/\sigma_r)^4$ as p grows.

5. Numerical experiments. The numerical evaluation of our randomized algorithms is comprised of three experiments: a simple multivariate linear regression to benchmark the bounds of Theorems 4.3 and 4.5, a large-scale vector-valued regression problem from computational neuroscience and a Koopman operator regression for a one-dimensional dynamical system, i.e., the noisy logistic map. In these large-scale problems, we are mainly interested in probing the enhanced performance of *randomized* reduced rank regression.

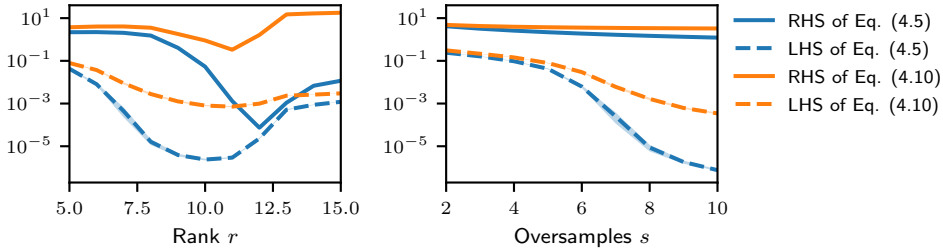


Figure 1. Comparison between the upper bounds (solid lines) derived in Theorems 4.3 and 4.5 and the estimated error (dashed lines) as a function of rank (left, $s = 5$) and of oversampling parameter s (right, $r = 5$). The estimated error is represented by the average ($\pm 95\%$ confidence interval) over 1000 independent seed initializations.

Linear system. We define a multivariate linear regression problem $Y = AX + \xi$ with $X = \{x_1, \dots, x_n\}$, $x_i \in \mathbb{R}^d$, $x_i \sim \mathcal{N}(0, I)$, $A \in \mathbb{R}^{d \times d}$ and $\xi \sim \mathcal{N}(0, \text{diag}(\text{std}))$ standard Gaussian random vectors. We designed a low-rank matrix $A = U\Sigma U^\top$ with U being a random orthogonal matrix $\in \mathbb{R}^{d \times d}$ and $\Sigma := \text{diag}(\sigma_1, \dots, \sigma_d) \in \mathbb{R}^{d \times d}$. The singular values are defined as $\sigma_i := 1/(1 + \exp(-z_i))$, where $z = r - (1, \dots, d)/\tau$, with r being the number of singular values close to 1 and τ being the decay length representing the number of singular values lying in the slope part of the sigmoid curve approaching 0.

For our numerical experiments, we set $d = 100$, $r = 10$, $\tau = 5$, $\text{std} = 0.1$, the number of training and test points $n = 1000$ and let $\psi(x) = \phi(x) = x$ for all $x \in \mathcal{X}$. We trained reduced rank estimators (2.2) both with the method as implemented in [16], based on Arnoldi iterations (R^3), and the method described in the present work, based on randomized SVD techniques (R^4). Each estimator was trained by fixing the regularization parameter $\gamma = 10^{-6}$ and the number of powering iterations $p = 1$.

In Fig. 1 we compare the actual value of $\mathbb{E}[\mathcal{R}^\gamma(\mathbf{A}_{r,\gamma}^{s,p})] - \mathcal{R}^\gamma(\mathbf{A}_{r,\gamma})$ against the upper bounds derived in Theorems 4.3 and 4.5 and we can appreciate how the empirical quantities are well below the theoretical bounds. The left panel shows the comparison conducted by varying the rank while keeping the oversampling parameter s fixed at 5. Conversely, the right panel shows the influence of the oversampling parameter s with rank set to 5.

Moreover, in Fig. 2 we compare risk and fit time of R^3 and R^4 algorithms as a function of the training sample size n . The estimators were trained with the parameters $r = 15$, $\gamma = 10^{-6}$ and, concerning R^4 , $p = 1$ and $s = 20$. We observe that the risk difference between R^4 and R^3 estimators on training data decreases as n increases and for test data is virtually 0 (left and center panels, respectively). This empirically suggests that the inaccuracies introduced by the randomized procedure do not affect the generalization performances of the estimator. Further, our naïve Python implementation attains, on average, a $\sim 8.6\times$ faster computation speed compared w.r.t. the highly optimized Arnoldi iterations implemented in the SciPy [34] package (right panel).

Large scale neuroscience dataset. To further prove the effectiveness of R^4 , we challenge it on a large scale neuroscience task: the Natural Scenes Dataset (NSD) [1, 12]. This dataset comprises high-resolution fMRI recordings obtained from 8 healthy subjects, each exposed to

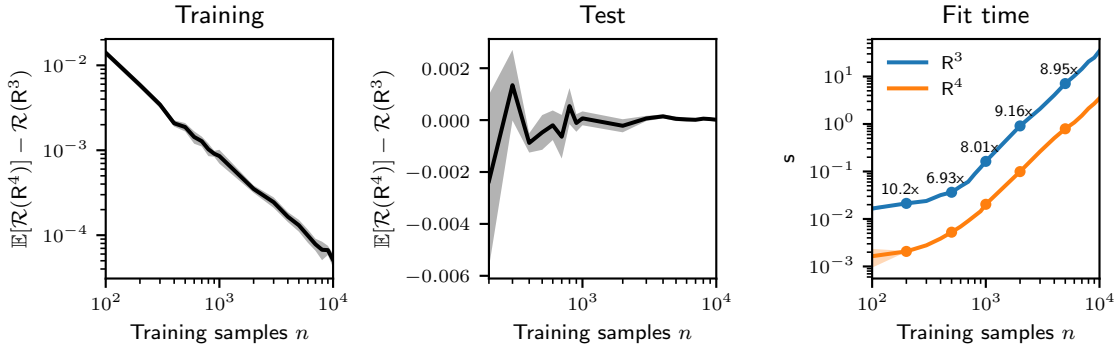


Figure 2. Risk difference evaluated on the training (left) and test (center) sets, and comparison of fit time between R^4 and R^3 (right). The estimated quantities are represented by the average over 10 independent seed initializations.

a set of 10000 images. Among these images, drawn from the COCO dataset [18], 9000 were unique stimuli and 1000 were shared across subjects. This provided us with a total of 73000 unique recording/stimulus pairs. The goal, here, is to assess the ability of our algorithm to predict the neural activity evoked by intricate natural visual stimuli.

We face this problem by learning separate reduced rank estimators $\mathbf{A}_{r,\gamma}$ for each subject and hemisphere. Each estimator acts as a mapping between the two high-dimensional input (images) space, where each image was described by several features (i.e., image embedding), and the output (fMRI) space, described by 19004 and 20544 vertices, respectively, for left and right hemisphere (except for subjects 6 and 8 which have 20220 and 20530 vertices respectively for the right hemisphere). To obtain a compact representation of the visual stimuli, we derive image embeddings from the last convolutional layer (`features.12`) of the well-known AlexNet model [17] (9216-dimensional feature vector), and from the recent computer vision foundation model DINOv2 (ViT-g) [24]. Concerning DINOv2, we follow the approach outlined in [6], which consists in concatenating the output of the [CLS] token and the GeM-pooled [28] output patch tokens from the last 20 blocks. This yields a 61440-dimensional feature vector for DINOv2, which, when combined with the one obtained from AlexNet, produces a 70565-dimensional image embedding.

In this experiment, we trained the estimators R^3 and R^4 with two different kernel combinations: (i) a linear kernel applied to both input and output spaces, and (ii) a Matérn kernel (with smoothness parameter $\nu = 0.5$) for the input space and a linear kernel for the output space. The estimators' performance was evaluated and compared in terms of mean Pearson's correlation (r), mean squared correlation r^2 , and mean noise-normalized squared correlation (NNSC, i.e., the challenge's metric described in [12]), computed over all the vertices from all subjects.

The hyperparameters of each estimator were tuned through a grid-search procedure using an independent validation set. The tuned hyperparameters were:

- the regularization parameter $\gamma \in [10^{-5}, 10^{-2}]$,
- the length-scale of Matérn kernel, selected from a set of quantiles (0.05, 0.25, 0.5,

Table 1

Comparison between baseline, R^3 and R^4 models in terms of Pearson’s correlation (r), squared correlation (r^2) and noise-normalized squared correlation (NNSC). Models are tested with private and challenge test sets. For R^4 models, hyperparameter optimization (HPO) is based on results obtained from a validation set of either R^3 (HPO: R^3) or R^4 (HPO: R^4). Best results are in bold.

Model	K_X	K_Y	HPO	Private test set			Challenge test set
				r	r^2	NNSC	NNSC
Baseline	/	/	/	0.3923	0.1816	55.172	47.639
R^3	Linear	Linear	R^3	0.4105	0.1993	59.537	51.749
R^4	Linear	Linear	R^3	0.4101	0.1988	59.443	51.637
R^4	Linear	Linear	R^4	0.4101	0.1989	59.424	51.634
R^3	Matérn	Linear	R^3	0.4147	0.2015	61.182	52.951
R^4	Matérn	Linear	R^3	0.4142	0.2010	61.024	52.828
R^4	Matérn	Linear	R^4	0.4142	0.2011	61.023	52.843

0.75, 0.95) derived from the pairwise distances among 1000 randomly selected image embeddings within the training set.

In Table 1, we show the results of the reduced rank estimators and a baseline model. As in [12], the baseline model consists of (i) a dimensionality reduction phase of the image embeddings to 100 dimensions through PCA, and (ii) learning a linear regression model between the reduced input and each single vertex. Notably, the learned reduced rank estimators effectively capture a (low-dimensional) mapping that links visual stimuli to the full fMRI activity, whereas the baseline model, following a univariate approach, neglects any relationship among vertices. This is reflected in the results where our (simple) approach outperforms the baseline model and, in particular, R^3 model with Matérn kernel applied on the input space achieves the best performance, ranking 21st out of 94 (at the moment of submission) in the post-challenge leaderboard (see Table 1). Moreover, the table reveals that for the same kernel choice, R^3 performs only slightly better than R^4 but at a significantly higher computational cost (see Fig. 3). Given the high dimensionality of the problem, both in terms of sample size and number of features, we implemented R^3 and R^4 algorithms using PyTorch [26] package to exploit GPU acceleration. This translates into a dramatic speedup of about three orders of magnitude (see Fig. 3, right panel).

Noisy logistic map. In the context of dynamical systems, our methodology can be employed to learn a low-rank approximation of the Koopman operator [16] associated to a dynamical system. We demonstrate how R^4 can achieve comparable performance to R^3 in approximating the Koopman operator from data, with a specific focus on eigenvalue estimation. We analyze the noisy logistic map, defined as $x_{t+1} = (4x_t(1 - x_t) + \xi_t) \bmod 1$ where $\mathcal{X} = [0, 1]$ and ξ_t is an i.i.d. trigonometric noise [25]. For the numerical experiment, we generate trajectories of 5000 and 10000 points as validation and test sets, respectively, with parameter N of the trigonometric noise set to 20. We set the target rank $r = 3$, the oversampling parameter $s = 20$, number of powering iterations $p = 1$ and regularization $\gamma = 10^{-7}$.

In Fig. 4 (left panel), we show the three leading eigenvalues $\lambda = \{1, -0.193 \pm 0.191i\}$ characterizing the Koopman operator of the noisy logistic map, and the eigenvalues estimated from R^3 and R^4 . To quantitatively assess whether the eigenvalues of the logistic map

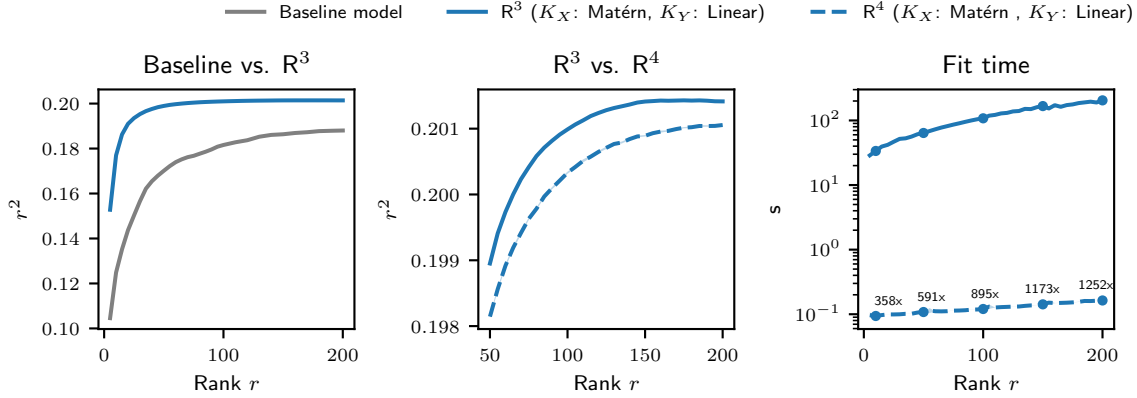


Figure 3. Assessment of the performance in predicting fMRI activity in terms of squared correlation, r^2 (the higher the better), and fit time. We show r^2 for baseline and R³ (left), R³ and R⁴ (center), and the fit time for R³ and R⁴ (right). The estimated quantities are represented by the average over 10 independent seed initializations.

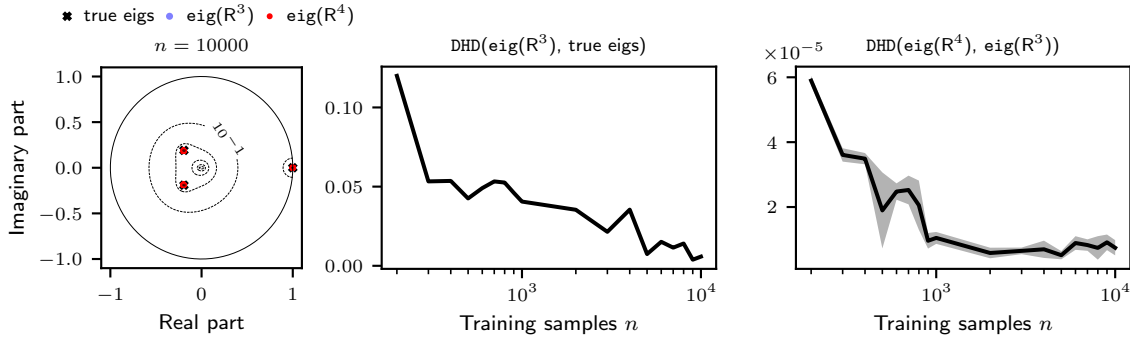


Figure 4. True and estimated eigenvalues of the logistic map (left), DHD between R³ estimated eigenvalues and true eigenvalues (center), and DHD between R³ and R⁴ estimated eigenvalues.

are well estimated, we used the *directed* Hausdorff distance (DHD) defined as $h(P, R) = \max_{p \in P} \min_{r \in R} |p - r|$, measuring the distance between a set P and a reference set R . We show that the DHD between the estimated eigenvalues with R³ and the true eigenvalues tend to zero as the training sample size increases (center panel). Remarkably, the estimated eigenvalues with R⁴ are virtually the same as the ones estimated with R³ (right panel).

6. Conclusions. We devised an efficient method to solve vector-valued regression problems by learning reduced rank estimators via a randomized algorithm. The numerical experiments confirmed the theoretical findings showing how R⁴ virtually attains the same accuracy of classical reduced rank regression being dramatically faster when dealing with real-world, large scale datasets.

An important open question for future research is how to combine the results of this work with statistical learning rates. This would unveil to which extent the computational com-

plexity of reduced rank regression can be reduced without deterioration of its generalization properties. Other interesting paths include combining our results with different strategies, such as Nyström subsampling [31] or random features [29], to further reduce the computational complexity of estimators, as well as addressing other vector-valued regression problems beyond the square loss.

REFERENCES

- [1] E. J. ALLEN, G. ST-YVES, Y. WU, J. L. BREEDLOVE, J. S. PRINCE, L. T. DOWDLE, M. NAU, B. CARON, F. PESTILLI, I. CHAREST, J. B. HUTCHINSON, T. NASELARIS, AND K. KAY, *A massive 7t fMRI dataset to bridge cognitive neuroscience and artificial intelligence*, *Nature Neuroscience*, 25 (2021), pp. 116–126, <https://doi.org/10.1038/s41593-021-00962-x>, <https://doi.org/10.1038/s41593-021-00962-x>.
- [2] A. ARGYRIOU, T. EVGENIOU, AND M. PONTIL, *Convex multi-task feature learning*, *Machine Learning*, 73 (2008), pp. 243–272.
- [3] N. ARONSZAJN, *Theory of reproducing kernels*, *Transactions of the American mathematical society*, 68 (1950), pp. 337–404.
- [4] S. BOYD AND L. VANDENBERGHE, *Convex Optimization*, Cambridge University Press, Mar. 2004, <https://doi.org/10.1017/cbo9780511804441>, <http://dx.doi.org/10.1017/CBO9780511804441>.
- [5] L. BROGAT-MOTTE, A. RUDI, C. BROUARD, J. ROUSU, AND F. D’ALCHÉ BUC, *Vector-valued least-squares regression under output regularity assumptions*, *Journal of Machine Learning Research*, 23 (2022), pp. 1–50.
- [6] M. CARON, H. TOUVRON, I. MISRA, H. JÉGOU, J. MAIRAL, P. BOJANOWSKI, AND A. JOULIN, *Emerging properties in self-supervised vision transformers*, in *Proceedings of the IEEE/CVF International Conference on Computer Vision (ICCV)*, October 2021, pp. 9650–9660.
- [7] L. CELLA, K. LOUNICI, G. PACREAU, AND M. PONTIL, *Multi-task representation learning with stochastic linear bandits*, in *International Conference on Artificial Intelligence and Statistics*, PMLR, 2023, pp. 4822–4847.
- [8] R. CHEN, H. XIAO, AND D. YANG, *Autoregressive models for matrix-valued time series*, *Journal of Econometrics*, 222 (2021), pp. 539–560.
- [9] C. CILIBERTO, L. ROSASCO, AND A. RUDI, *A general framework for consistent structured prediction with implicit loss embeddings*, *Journal of Machine Learning Research*, 21 (2020), pp. 1–67, <http://jmlr.org/papers/v21/20-097.html>.
- [10] F. DINUZZO AND K. FUKUMIZU, *Learning low-rank output kernels*, in *Asian Conference on Machine Learning*, PMLR, 2011, pp. 181–196.
- [11] Y. DIOUANE, S. GÜROL, A. S. DI PERROTOLO, AND X. VASSEUR, *A general error analysis for randomized low-rank approximation methods*, 2022, <https://doi.org/10.48550/ARXIV.2206.08793>, <https://arxiv.org/abs/2206.08793>.
- [12] A. T. GIFFORD, B. LAHNER, S. SABA-SADIYA, M. G. VILAS, A. LASCELLES, A. OLIVA, K. KAY, G. ROIG, AND R. M. CICHY, *The algonauts project 2023 challenge: How the human brain makes sense of natural scenes*, 2023, <https://doi.org/10.48550/ARXIV.2301.03198>, <https://arxiv.org/abs/2301.03198>.
- [13] Y. IDELBAYEV AND M. A. CARREIRA-PERPINÁN, *Low-rank compression of neural nets: Learning the rank of each layer*, in *Proceedings of the IEEE/CVF Conference on Computer Vision and Pattern Recognition*, 2020, pp. 8049–8059.
- [14] A. J. IZENMAN, *Reduced-rank regression for the multivariate linear model*, *Journal of multivariate analysis*, 5 (1975), pp. 248–264.
- [15] T. KATO, *Perturbation Theory for Linear Operators*, 1966.
- [16] V. KOSTIC, P. NOVELLI, A. MAURER, C. CILIBERTO, L. ROSASCO, AND M. PONTIL, *Learning dynamical systems via koopman operator regression in reproducing kernel hilbert spaces*, *Advances in Neural Information Processing Systems*, 35 (2022), pp. 4017–4031.
- [17] A. KRIZHEVSKY, I. SUTSKEVER, AND G. E. HINTON, *ImageNet classification with deep convolutional neu-*

- ral networks*, Communications of the ACM, 60 (2017), pp. 84–90, <https://doi.org/10.1145/3065386>, <https://doi.org/10.1145/3065386>.
- [18] T.-Y. LIN, M. MAIRE, S. BELONGIE, J. HAYS, P. PERONA, D. RAMANAN, P. DOLLÁR, AND C. L. ZITNICK, *Microsoft COCO: Common objects in context*, in Computer Vision – ECCV 2014, Springer International Publishing, 2014, pp. 740–755, https://doi.org/10.1007/978-3-319-10602-1_48, https://doi.org/10.1007/978-3-319-10602-1_48.
- [19] G. LUISE, D. STAMOS, M. PONTIL, AND C. CILIBERTO, *Leveraging low-rank relations between surrogate tasks in structured prediction*, in International Conference on Machine Learning, PMLR, 2019, pp. 4193–4202.
- [20] P.-G. MARTINSSON AND J. A. TROPP, *Randomized numerical linear algebra: Foundations and algorithms*, Acta Numerica, 29 (2020), pp. 403–572, <https://doi.org/10.1017/s0962492920000021>, <https://doi.org/10.1017/s0962492920000021>.
- [21] M. MOLLENHAUER, N. MÜCKE, AND T. SULLIVAN, *Learning linear operators: Infinite-dimensional regression as a well-behaved non-compact inverse problem*, arXiv preprint arXiv:2211.08875, (2022).
- [22] M. MOLLENHAUER, I. SCHUSTER, S. KLUS, AND C. SCHÜTTE, *Singular value decomposition of operators on reproducing kernel hilbert spaces*, in Advances in Dynamics, Optimization and Computation: A volume dedicated to Michael Dellnitz on the occasion of his 60th birthday, Springer, 2020, pp. 109–131.
- [23] A. MUKHERJEE AND J. ZHU, *Reduced rank ridge regression and its kernel extensions*, Statistical Analysis and Data Mining: The ASA Data Science Journal, 4 (2011), p. 612–622, <https://doi.org/10.1002/sam.10138>, <http://dx.doi.org/10.1002/sam.10138>.
- [24] M. OQUAB, T. DAR CET, T. MOUTAKANNI, H. VO, M. SZA FRANIEC, V. KHALIDOV, P. FERNANDEZ, D. HAZIZA, F. MASSA, A. EL-NOUBY, M. ASSRAN, N. BALLAS, W. GALUBA, R. HOWES, P.-Y. HUANG, S.-W. LI, I. MISRA, M. RABBAT, V. SHARMA, G. SYNNAEVE, H. XU, H. JEGOU, J. MAIRAL, P. LABATUT, A. JOULIN, AND P. BOJANOWSKI, *Dinov2: Learning robust visual features without supervision*, 2023, <https://doi.org/10.48550/ARXIV.2304.07193>, <https://arxiv.org/abs/2304.07193>.
- [25] A. OSTRUSZKA, P. PAKOŃSKI, W. SŁOMCZYŃSKI, AND K. ŻYCZKOWSKI, *Dynamical entropy for systems with stochastic perturbation*, Physical Review E, 62 (2000), p. 2018–2029, <https://doi.org/10.1103/physreve.62.2018>, <http://dx.doi.org/10.1103/PhysRevE.62.2018>.
- [26] A. PASZKE, S. GROSS, F. MASSA, A. LERER, J. BRADBURY, G. CHANAN, T. KILLEEN, Z. LIN, N. GIMELSHEIN, L. ANTIGA, ET AL., *Pytorch: An imperative style, high-performance deep learning library*, Advances in neural information processing systems, 32 (2019).
- [27] G. RABUSSEAU AND H. KADRI, *Low-rank regression with tensor responses*, Advances in Neural Information Processing Systems, 29 (2016).
- [28] F. RADENOVIC, G. TOLIAS, AND O. CHUM, *Fine-tuning cnn image retrieval with no human annotation*, IEEE Transactions on Pattern Analysis and Machine Intelligence, 41 (2019), p. 1655–1668, <https://doi.org/10.1109/tpami.2018.2846566>, <http://dx.doi.org/10.1109/TPAMI.2018.2846566>.
- [29] A. RAHIMI AND B. RECHT, *Random features for large-scale kernel machines*, Advances in Neural Information Processing Systems, 20 (2007).
- [30] G. C. REINSEL, R. P. VELU, AND K. CHEN, *Multivariate Reduced-Rank Regression: Theory, Methods and Applications*, vol. 225, Springer Nature, 2022.
- [31] A. RUDI, R. CAMORIANO, AND L. ROSASCO, *Less is more: Nyström computational regularization*, Advances in Neural Information Processing Systems, 28 (2015).
- [32] L. SONG, J. HUANG, A. SMOLA, AND K. FUKUMIZU, *Hilbert space embeddings of conditional distributions with applications to dynamical systems*, in Proceedings of the 26th Annual International Conference on Machine Learning - ICML '09, ACM Press, 2009, <https://doi.org/10.1145/1553374.1553497>, <https://doi.org/10.1145/1553374.1553497>.
- [33] J. A. TROPP, A. YURTSEVER, M. UDELL, AND V. CEVHER, *Practical sketching algorithms for low-rank matrix approximation*, SIAM Journal on Matrix Analysis and Applications, 38 (2017), pp. 1454–1485, <https://doi.org/10.1137/17m1111590>, <https://doi.org/10.1137/17m1111590>.
- [34] P. VIRTANEN, R. GOMMERS, T. E. OLIPHANT, M. HABERLAND, T. REDDY, D. COURNAPEAU, E. BUROVSKI, P. PETERSON, W. WECKESSER, J. BRIGHT, S. J. VAN DER WALT, M. BRETT, J. WILSON, K. J. MILLMAN, N. MAYOROV, A. R. J. NELSON, E. JONES, R. KERN, E. LARSON, C. J. CAREY, İ. POLAT, Y. FENG, E. W. MOORE, J. VANDERPLAS, D. LAXALDE, J. PERK-

TOLD, R. CIMRMAN, I. HENRIKSEN, E. A. QUINTERO, C. R. HARRIS, A. M. ARCHIBALD, A. H. RIBEIRO, F. PEDREGOSA, P. VAN MULBREGT, AND SCI-PY 1.0 CONTRIBUTORS, *SciPy 1.0: Fundamental Algorithms for Scientific Computing in Python*, Nature Methods, 17 (2020), pp. 261–272, <https://doi.org/10.1038/s41592-019-0686-2>.